

Communication

# Fabrication and Characterization of Porous Copper with Ultrahigh Porosity

Jian Xiao <sup>\*</sup>, Yong Li, Jinming Liu and Qianlei Zhao <sup>\*</sup>

Faculty of Materials Metallurgy and Chemistry, Jiangxi University of Science and Technology, Ganzhou 341000, China; liyong0248@163.com (Y.L.); liujm2011@jxust.edu.cn (J.L.)

<sup>\*</sup> Correspondence: xiaojian@jxust.edu.cn (J.X.); zhaoqianlei@jxust.edu.cn (Q.Z.)

**Abstract:** The fabrication of porous copper with ultrahigh porosity by adding 90% spacer content was an unsolved technical problem in the field. In this study, the green compacts placed on a layer wire mesh during the decomposition process of needlelike carbamide as space holder with volume content up to 90% was successfully conducted to fabricate nondestructive porous copper. Compared with the green compacts directly placed on an alumina plate, the use of this support was crucial for manufacturing highly-porous copper. Characterization of macro- and microscopic morphologies as well as quasi-static compressive test for the obtained porous copper samples was carried out. The results show that the porosity of porous copper samples with 87.3% was slightly smaller than the spacer content. The SEM observation indicates that the internal pores of porous copper formed an open-cell structure and its skeleton was very dense. The compressive tests show that the stress–strain curve of a porous copper sample exhibits the typical characteristics of elastic-plastic metal foam. The energy absorption properties of porous copper samples were also comparable. This study provides a possibility for the preparation of porous copper and other metals with ultrahigh porosity by the well-known space holder method.

**Keywords:** metal foam; porous metal; powder metallurgy; space holder; ultrahigh porosity



**Citation:** Xiao, J.; Li, Y.; Liu, J.; Zhao, Q. Fabrication and Characterization of Porous Copper with Ultrahigh Porosity. *Metals* **2022**, *12*, 1263. <https://doi.org/10.3390/met12081263>

Academic Editor: Thomas Fiedler

Received: 23 June 2022

Accepted: 26 July 2022

Published: 27 July 2022

**Publisher's Note:** MDPI stays neutral with regard to jurisdictional claims in published maps and institutional affiliations.



**Copyright:** © 2022 by the authors. Licensee MDPI, Basel, Switzerland. This article is an open access article distributed under the terms and conditions of the Creative Commons Attribution (CC BY) license (<https://creativecommons.org/licenses/by/4.0/>).

## 1. Introduction

As a member in porous metals, porous copper was widely used in the fields of catalysis, energy, and analytical sensing due to the excellent electrical and thermal conductivity of copper metal [1]. The application of porous copper depends considerably on its pore structure design, which in turn depends on the preparation method. Space holder technique [2] and gas release reaction [3,4] were the two main powder metallurgy approaches used to fabricate porous copper. Since the porosity of the final materials can be predicted by the spacer content [2], the space holder technique has obtained increased attention. Zhao et al. [5] first described a lost potassium carbonate sintering process for manufacturing open-cell copper foams with porosity in the range of 50–85% and cell sizes in the range of 53–1500  $\mu\text{m}$  in 2004. This structural characteristic of porous copper immediately aroused a new research interest and new space holders are being discovered. For example, Wang et al. [6] reported that an open-cell porous copper with adjustable pore characteristics and mechanical properties has been successfully prepared using sodium chloride as space holder via the sintering-dissolution process for the first time. Stergioudi et al. [7] reported that open-cell copper foams were prepared using sugar as space holder technique and tested as filter-bed for the uptake and reduction of Cr in drinking water. Moreover, Zhao et al. [8] reported that open-porous Cu-Sn-Ti composites are fabricated by the space holder sintering technique using carbamide particles as space holder material. The following literatures related to potassium carbonate [9], sodium chloride [10], and carbamide [11] demonstrated that the final porosity of porous copper was strongly dependent on the volume content of space holder added. Generally, the higher the spacer content, the higher

the porosity. However, the more difficult it is to prepare. The majority of the space holders reported in literatures can reach 80%, a few up to 85%, and almost, but not up to 90%. It was believed that at this high content, the removal of space holder leads to the collapse of the powder compact [7,12]. At this high spacer content, how to avoid the collapse of green compacts during the removal process of space holder particles is a great challenge. As a result, the structure and properties of porous copper with 90% of volume content were unknown. Therefore, this paper aims to try and use needlelike carbamide as space holder with volume content up to 90% to prepare porous copper with ultrahigh porosity, since carbamide was often used to create desirable pore geometries and porosities into porous copper due to its low-temperature decomposition during the sintering process [13,14]. We hope that it can provide a new idea for the preparation of porous copper with ultrahigh porosity by the space holder technique.

## 2. Materials and Methods

### 2.1. Materials

High purity Cu powder (~99.9%, supplied by Beijing Hongyu New Material Technology Co., Ltd., Beijing, China) with irregular shapes (see Figure 1a) and particle size less than 50  $\mu\text{m}$  as received was used as raw material. The needlelike carbamide (see Figure 1b) purchased from Xilong Scientific Co., Ltd. (Shantou, China) was selected after a sieve was passed with 40–80 mesh (~180–380  $\mu\text{m}$ ) as space holder. The volume fraction of space holder was set as 90% and the total volume of copper powder and carbamide was determined based on a cylinder with 20 mm in diameter and 8 mm in height.

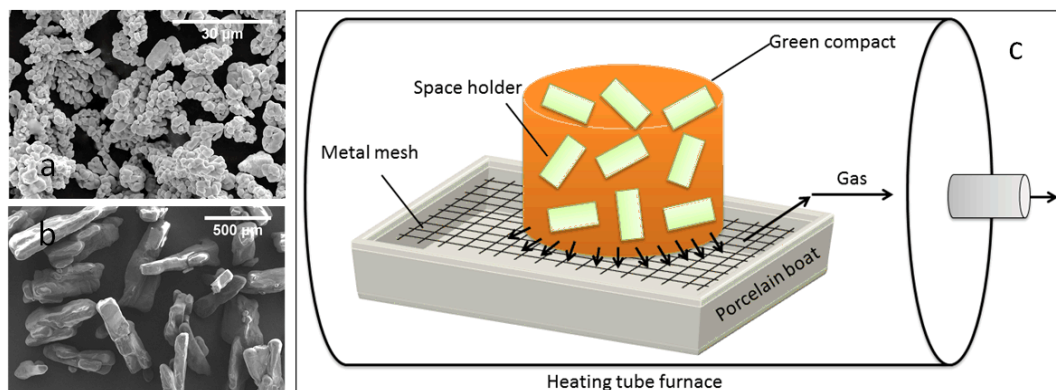


**Figure 1.** SEM images of (a) copper powder and (b) carbamide particles. (c) Schematic diagram of a green compact placed on a layer of metal mesh support in porcelain boat during the decomposition process of space holder in a heating tube furnace.

### 2.2. Methods

Initially, the weighed copper powder and carbamide were mixed evenly for some time, then the mixture was followed by compaction with a pressure of 200 MPa and maintained for 0.5 min. Thereafter, the heat treatment of green compacts was carried out in two steps. First, the green compacts were transferred into a tubular vacuum furnace (KEJING Company, Shenyang, China) after they were placed on a layer of wire mesh in a burning boat (for its schematic diagram, see Figure 1c). The green compacts were heated to 673 K for 300 min. As a result, a porous Cu bulk was obtained successfully after it was cooled down to room temperature. The first step is to remove the carbamide particles in the preform and maintain the sintering temperature at a low temperature. Second, the Cu compacts without carbamide, herein named preheated samples after the same compaction process, were fabricated after being heated to 1123 K at  $10\text{ }^{\circ}\text{C min}^{-1}$  in the tubular vacuum furnace and cooled down to room temperature for comparison. The second step was to promote metallurgical bonding between copper particles by diffusion. The external dimensions of three porous copper samples with 18.3 mm in diameter and 7.54 mm in

height were measured. The porosities of samples were measured and calculated by the model equation method [15]. Their surface morphologies were observed using a scanning electron microscope (FEI Company, Hillsboro, OR, USA). The compressive tests were carried out on an electronic universal testing machine (SUNS Company, Shenzhen, China) with a crosshead speed of  $1 \text{ mm min}^{-1}$  at room temperature ( $\sim 25 \text{ }^\circ\text{C}$ ), according to ISO 13314-11 standard [16]. To obtain reproducibility of the results, three valid results were considered and used to calculate the average properties of the obtained porous copper samples.

### 3. Results and Discussion

In general, the green compacts were directly placed on an alumina plate (see Figure 2a). However, the result shows that the compacts completely collapsed with removal time of 200 min (white arrow-I). This indicates that the heating rate has an important influence on the removal effect of green compacts. When the removal time increases to 300 min, large defects at the bottom of sintered compacts can be seen although it does not completely collapse (white arrow-II). These defects emerged from the gas escape process in the green compacts. When the removal time further increases to 400 min, the result shows that the defects changed from large to small (white arrow-III). After researching the essential problem, the gas produced by thermal decomposition of carbamide near alumina plate has no time to escape from the compacts. In addition, when the compacts were placed on a metal mesh support (see Figure 2b), the result shows that the compacts remained in their shapes even when the removal time increases to 300 min (orange arrow). It can be seen that the influence of metallic mesh on removal kinetics is rather major, since the products of carbamide decomposition evaporate in the direction of mesh. In this way, nondestructive porous copper samples were successfully obtained.

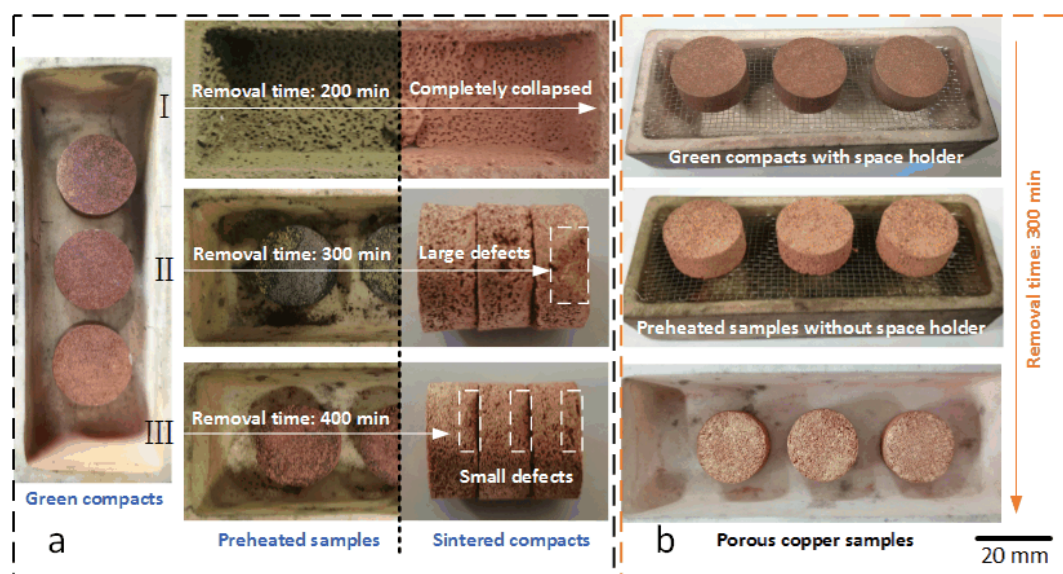


**Figure 2.** Comparison in thermal removal results of green compacts placed on different substrates: (a) An alumina plate and (b) a layer metal mesh.

The top surface SEM images of a nondestructive porous copper sample with porosity of 87.3% calculated by model equation method shows that there are large numbers of pores, which can be clearly seen in Figure 2a. These pores known as macropores were generated from the thermal removal of carbamide particles. They are interconnected to form an open structure. Their shape is even more irregular although some pores retain the shape of space holder. The length and width of pore sizes were about  $548 \pm 201 \mu\text{m}$  and  $177 \pm 62 \mu\text{m}$ , respectively. It can be seen that the length of pore sizes was significantly larger than a single carbamide particle. This phenomenon was attributed to the fact that multiple carbamide particles were next to each other in green compacts and the holes they

leave behind form a larger pore. On the other hand, the width of pore sizes was slightly lower than a single carbamide particle. This phenomenon was attributed to the volumetric shrinkage of holes generated from the removal of space holder during sintering. Through local magnification, it can be seen that the skeleton is dense, but it also contains some black spots (see Figure 3b). The thickness of the cell walls was about  $12.8 \pm 0.4 \mu\text{m}$ . The black spots known as micropores were produced as a secondary effect of incomplete densification of the sintered copper particles. They are scattered sporadically across the skeleton in small numbers at higher magnification (see Figure 3c). The metal skeleton was generated from the diffusion and sintering of copper powders. They gradually become round and sharp and their surface changes from rough to smooth after sintering. The sintered necks were coarse and uniform with a good metallurgical bonding, which can be clearly seen at higher magnification in Figure 3d.

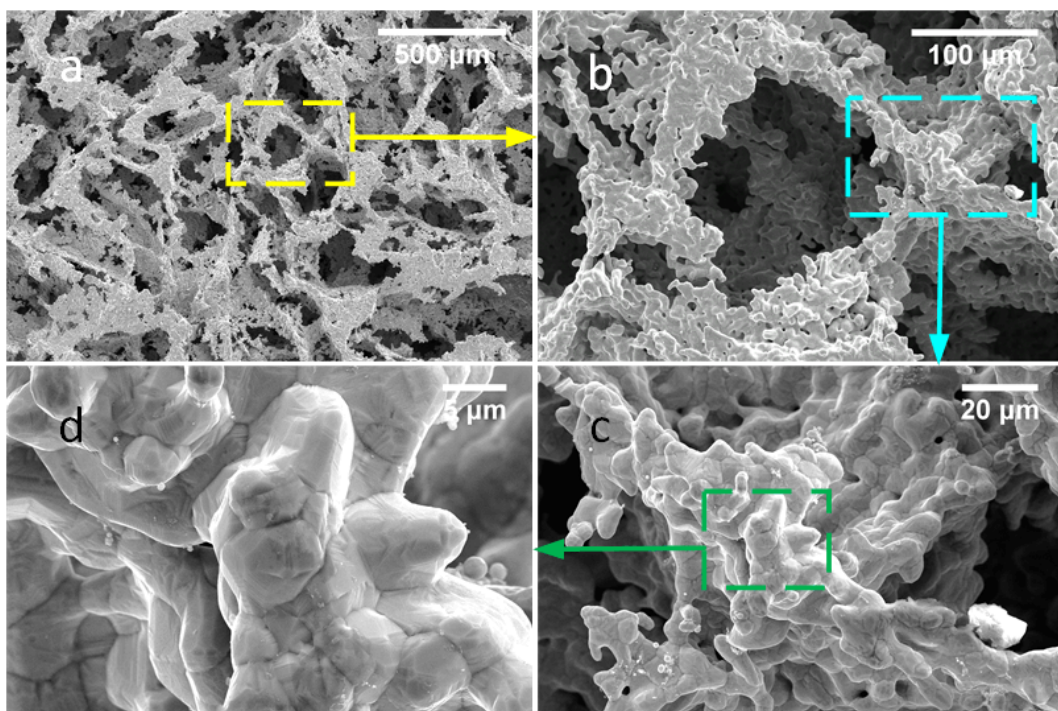


**Figure 3.** Top surface SEM images of a nondestructive porous copper sample taken at different magnifications: (a) 200, (b) 1000, (c) 3000, and (d) 10,000.

The nominal stress–strain curves of three porous copper samples by axial compressive test were shown in Figure 4a. Herein, the compressive stress was the compressive force divided by the initial cross-sectional area perpendicular to the loading direction. The compressive strain was the overall compressive displacement divided by the initial height (gauge length) of the test specimen. It can be seen that the curves exhibit the typical characteristics of elastic–plastic metal foam [17–21]: The linear elastic deformation at initial region, plastic deformation at plateau region, and further compaction deformation increases rapidly at densification region. Meanwhile, the three curves were highly coincident, which indicates that the quality uniformity of the specimens was perfect. The elastic modulus can be calculated from the slope of the linear line at the initial stage of stress–strain curve and the yield strength was 0.2% of the elastic limit residual deformation since there was no clear yield point. During the plateau region, the main collapse mechanisms (e.g., bending or yielding of the cell walls, brittle fracture of cell walls, buckling of thin walls, etc.) in foams occur [22,23]. According to ISO 13314-11 standard [16], the plateau strength was calculated as the arithmetical mean of the stresses between 20% and 40% compressive strains. The densification region contains the compaction of the cells with a steep and nearly linear increase in stress and the most important aspect of this region is the strain

in which densification starts [19]. However, the compressive stress corresponding to the first local maximum in the stress–strain curve cannot be determined since no local maximum occurs, as shown in Figure 4a. In this case, the energy absorption properties can be used to derive compressive strength and densification strain. The energy absorption capacity was defined as the energy required to deform the sample to a specific strain and can be evaluated by integrating the area under the stress–strain curve [24], as shown in Figure 4b. The maximum capacity was obtained at densification strain and this value can be determined by energy absorption efficiency–stress curve (see Figure 4c). The energy absorption efficiency was the ratio of absorbed energy to the corresponding stress. The stress corresponding to the maximum energy absorption efficiency is the compressive strength, as shown in Figure 4c. In this way, the strain corresponding to compressive strength can be found in stress–strain curve. Then, the value corresponding to the above densification strain was the maximum energy absorption capacity, as shown in Figure 4b.

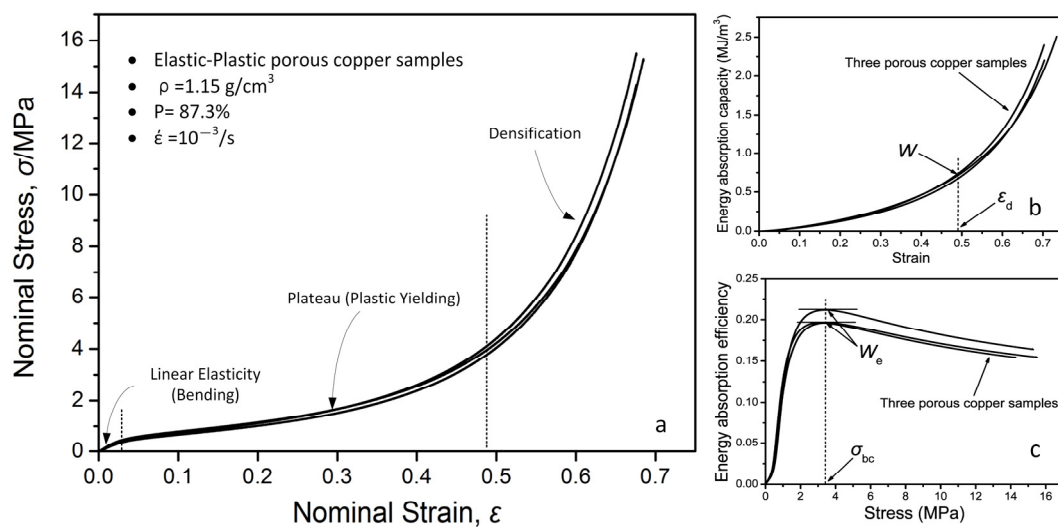


**Figure 4.** Mechanical curves of the samples: (a) Stress–strain, (b)  $W$ -strain, (c)  $W_e$ -stress.

The mean values with their standard deviations of mechanical properties of the obtained porous copper samples were calculated and shown in Table 1. Herein,  $E$ -Elastic is modulus;  $\sigma_{ys}$  is yield strength;  $\sigma_{pl}$  is plateau strength;  $\sigma_{bc}$  is compressive strength, which was the stress corresponding to the maximum energy absorption efficiency;  $\epsilon_d$  is densification strain;  $W$  is energy absorption capacity; and  $W_e$  is energy absorption efficiency. The average elastic modulus, yield strength, plateau strength, compressive strength, densification strain, energy absorption capacity, and energy absorption efficiency of three porous copper samples were calculated to be about  $13.80 \pm 2.22 \text{ MPa}$ ,  $0.33 \pm 0.03 \text{ MPa}$ ,  $1.64 \pm 0.11 \text{ MPa}$ ,  $3.33 \pm 0.22 \text{ MPa}$ ,  $48\% \pm 1\%$ ,  $0.69 \pm 0.06 \text{ MJ/m}^3$ ,  $20.33 \pm 0.58\%$ , respectively. In recent work [25], the energy absorption value of the reticulated copper foams with 87.7% porosity was  $0.39 \text{ MJ/m}^3$ . Comparatively, the porous copper prepared in this study has a stronger energy absorption capacity.

**Table 1.** The mechanical properties of the obtained three porous copper samples.

Sample Numbers	$E/\text{MPa}$	$\sigma_{ys}/\text{MPa}$	$\sigma_{pl}/\text{MPa}$	$\sigma_{bc}/\text{MPa}$	$\epsilon_d/\%$	$W/\text{MJ}\cdot\text{m}^{-3}$	$W_e/\%$
1#	16.34	0.35	1.55	3.45	49	0.75	21
2#	12.86	0.30	1.76	3.07	47	0.62	20
3#	12.21	0.33	1.62	3.46	48	0.70	20
Mean values	13.80	0.33	1.64	3.33	48	0.69	20.33
Standard deviations	2.22	0.03	0.11	0.22	1	0.06	0.58

#### 4. Conclusions

In this study, an open-cell structure of porous Cu with a porosity of 87.3% was prepared successfully via a decomposition–sintering route. As a space holder, carbamide with volume content up to 90% in the Cu compact can be removed completely during the sintering process by heating to 673 K within 300 min in vacuum atmosphere. The porous Cu is composed of interconnected pore structures and dense skeletons, indicating that the bonding between Cu powders can be achieved after the compacting of 200 MPa and sintering process of 1123 K. The compressive stress–strain curves of porous copper have typical characteristics of metal foam, and the repeatability of the curves of the three samples was very good. The average elastic modulus, yield strength, plateau strength, compressive strength, densification strain, energy absorption capacity, and energy absorption efficiency of three porous copper samples were calculated to be about  $13.80 \pm 2.22$  MPa,  $0.33 \pm 0.03$  MPa,  $1.64 \pm 0.11$  MPa,  $3.33 \pm 0.22$  MPa,  $48\% \pm 1\%$ ,  $0.69 \pm 0.06$  MJ/m<sup>3</sup>,  $20.33 \pm 0.58\%$ , respectively. By comparison, the porous copper in this study has comparable energy absorption capacity.

**Author Contributions:** Conceptualization, J.X. and Q.Z.; methodology, J.X.; software, J.X.; validation, J.X. and Q.Z.; formal analysis, J.X.; investigation, J.X. and Q.Z.; resources, J.L., Y.L. and J.X.; data curation, J.X.; writing—original draft preparation, J.X. and Q.Z.; writing—review and editing, J.X. and Q.Z.; visualization, J.X. and Q.Z.; supervision, J.X.; project administration, J.L., J.X. and Q.Z. All authors have read and agreed to the published version of the manuscript.

**Funding:** This research was funded by the National Natural Science Foundation of China (grant number 51961014); the Education Department of Jiangxi Province (grant numbers GJJ200834 and S202110407009).

**Institutional Review Board Statement:** Not applicable.

**Informed Consent Statement:** Not applicable.

**Data Availability Statement:** Not applicable.

**Conflicts of Interest:** The authors declare no conflict of interest.

#### References

1. Li, Z.B.; Wang, J.; Liu, X.J.; Li, R.; Wang, H.; Wu, Y.; Wang, X.Z.; Lu, Z.P. Self-supported NiCoP/nanoporous copper as highly active electrodes for hydrogen evolution reaction. *Scr. Mater.* **2019**, *173*, 51–55. [[CrossRef](#)]
2. Xiao, J.; Cui, H.; Qiu, G.B.; Yang, Y.; Lyu, X.W. Investigation on relationship between porosity and spacer content of titanium foams. *Mater. Des.* **2015**, *88*, 132–137.
3. Yang, D.H.; Guo, S.S.; Chen, J.Q.; Lu, J.; Wang, L.; Jiang, J.H.; Ma, A.B. Fabrication of Cu-Mg alloy foam with close pore structure by gas release reaction powder metallurgical approach. *J. Alloy. Compd.* **2018**, *766*, 851–858. [[CrossRef](#)]
4. Wang, X.Z.; Meng, Q.X.; Wang, T.Z.; Chu, X.M.; Fan, A.Q.; Wang, H. New Insights into Fabrication of Al-Based Foam with Homogeneous Small Pore-Structure Using MgCO<sub>3</sub>/Zn Composite Powder as a Foaming Agent. *Metals* **2022**, *12*, 786. [[CrossRef](#)]
5. Zhao, Y.Y.; Fung, T.; Zhang, L.P.; Zhang, F.L. Lost carbonate sintering process for manufacturing metal foams. *Scr. Mater.* **2004**, *52*, 295–298. [[CrossRef](#)]
6. Wang, Q.Z.; Cui, C.X.; Liu, S.J.; Zhao, L.C. Open-celled porous Cu prepared by replication of NaCl space-holders. *Mater. Sci. Eng. A* **2010**, *527*, 1275–1278. [[CrossRef](#)]
7. Stergioudi, F.; Kaprara, E.; Simeonidis, K.; Sagris, D.; Mitrakas, M.; Vourlias, G.; Michailidis, N. Copper foams in water treatment technology: Removal of hexavalent chromium. *Mater. Des.* **2015**, *87*, 287–294. [[CrossRef](#)]
8. Zhao, B.; Yu, T.Y.; Ding, W.F.; Li, X.Y.; Su, H.H. BP neural network based flexural strength prediction of open-porous Cu-SnTi composites. *Prog. Nat. Sci. Mater. Int.* **2018**, *28*, 315–324. [[CrossRef](#)]
9. Mosalagae, M.; Renteria, C.M.B.; Elbadawi, M.; Shbeh, M.; Goodall, R. Structural characterisation of porous copper sheets fabricated by lost carbonate sintering applied to tape casting. *Mater. Charact.* **2020**, *159*, 110009. [[CrossRef](#)]
10. Wang, Q.Z.; Lu, D.M.; Cui, C.X.; Liang, L.M. Compressive behaviors and energy-absorption properties of an open-celled porous Cu fabricated by replication of NaCl space-holders. *J. Mater. Process. Technol.* **2011**, *211*, 363–367. [[CrossRef](#)]
11. Zhao, B.; Yu, T.Y.; Ding, W.F.; Zhang, L.C.; Su, H.H.; Chen, Z.Z. Effect of micropores on the microstructure and mechanical properties of porous Cu-Sn-Ti composites. *Mater. Sci. Eng. A* **2018**, *730*, 345–354. [[CrossRef](#)]
12. Xie, B.; Zhou, Y.; Guo, K.; Zhong, H.; Zuo, X. Microstructure and Mechanical Properties of Bronze Foams Prepared Using CaCl<sub>2</sub> as Space Holder. *Rare Met. Mater. Eng.* **2018**, *47*, 279–285.
13. Agbedor, S.O.; Yang, D.H.; Chen, J.Q.; Wang, L.; Wu, H. Low-Temperature Reactive Sintered Porous Mg-Al-Zn Alloy Foams. *Metals* **2022**, *12*, 692. [[CrossRef](#)]

14. Xiao, J.; Liu, Y.N.; Li, Y.; Qiu, G.B.; Liu, J.M. The application of model equation method in preparation of titanium foams. *J. Mater. Res. Technol.* **2021**, *13*, 121–127.
15. Xiao, J.; Qiu, G.B. A novel method to measure the porosity of porous materials. *Mater. Sci. Technol.* **2020**, *36*, 127–129.
16. *ISO13314; Mechanical Testing of Metals-Ductility Testing-Compression Test for Porous and Cellular Metals*. ISO: Switzerland Geneva, 2011.
17. Wang, H.; Li, R.; Wu, Y.; Chu, X.M.; Lu, Z.P. Plasticity improvement in a bulk metallic glass composed of an open-cell Cu foam as the skeleton. *Compos. Sci. Technol.* **2012**, *75*, 49–54. [[CrossRef](#)]
18. Movahedi, N.; Linul, E. Radial crushing response of ex-situ foam-filled tubes at elevated temperatures. *Compos. Struct.* **2021**, *277*, 634–647. [[CrossRef](#)]
19. Linul, E.; Khezzzadeh, O. Axial crashworthiness performance of foam-based composite structures under extreme temperature conditions. *Compos. Struct.* **2021**, *271*, 156–166. [[CrossRef](#)]
20. Orbulov, I.N.; Szlancsik, A.; Kemény, A.; Kincses, D. Compressive mechanical properties of low-cost, aluminium matrix syntactic foams. *Compos. Part A* **2020**, *135*, 923–933. [[CrossRef](#)]
21. Epasto, G.; Distefano, F.; Gu, L.; Mozafari, H.; Linul, E. Design and optimization of Metallic Foam Shell protective device against flying ballast impact damage in railway axles. *Mater. Des.* **2020**, *196*, 120–135. [[CrossRef](#)]
22. Rajak, D.K.; Linul, E. Crushing Response of Composite Metallic Foams: Density and High Strain Rate Effects. *J. Alloy. Compd.* **2021**, *871*, 614–922. [[CrossRef](#)]
23. Khezzzadeh, O.; Mirzaee, O.; Emadoddin, E.; Linul, E. Anisotropic Compressive Behavior of Metallic Foams under Extreme Temperature Conditions. *Materials* **2020**, *13*, 2329. [[CrossRef](#)] [[PubMed](#)]
24. Zhao, W.; He, S.Y.; Zhang, C.; Li, Y.X.; Zhang, Y.; Dai, G. Generation of a Strength Gradient in Al-Cu-Ca Alloy Foam via Graded Aging Treatment. *Metals* **2022**, *12*, 423. [[CrossRef](#)]
25. Sutygina, A.; Betke, U.; Scheffler, M. Hierarchical-Porous Copper Foams by a Combination of Sponge Replication and Freezing Techniques. *Adv. Eng. Mater.* **2021**, *24*, 2001516. [[CrossRef](#)]